Pis'ma v ZhETF, vol. 92, iss. 6, pp. 465 – 472

ПО ИТОГАМ ПРОЕКТОВ
РОССИЙСКОГО ФОНДА ФУНДАМЕНТАЛЬНЫХ ИССЛЕДОВАНИЙ
Проект РФФИ # 07-02-01196a

Colour effective particles and confinement

V. V. Anisovich

Petersburg Nuclear Physics Institute, 188300 Gatchina, Russia

Submitted 26 July 2010

A brief review of papers (grant RFBF-07-02-01197a) is presented. The idea is evolved that colour confinement is realized by a singular interaction at large distances between colour effective particles (constituent quarks, diquarks, massive effective gluons).

1. Constituent quarks as colour effective particles. The first successful steps in understanding the internal structure of hadrons were made in 60's by introducing the idea of constituent quarks, according to which baryons are three-quark systems and mesons are quark–antiquark ones. Non-relativistic description of these systems gave rise to the systematization of low-lying states ($SU(6)$ symmetry) and allowed one to work with constituent quarks being non-flying out objects due to a potential barrier. The weak point of this approach is its inapplicability to highly excited states. Later on, experimental and theoretical studies revealed more complicated structure of hadrons, with constituent quarks as spatially separated clusters of QCD particles. It allowed us to consider the constituent quark as an effective particle, i.e. a "dressed quark" of the valence QCD quark. For reactions at low and moderately high energies the masses of light constituent quarks ($q = u,\, d,\, s$) are of the order of $m_u \simeq m_d \simeq$ $\simeq 300{-}400\,\mathrm{MeV}$ and $m_s - m_u \simeq 150\,\mathrm{MeV}$. The size of the light constituent quark $\langle r^2_{\text{constituent quark}}\rangle \simeq 0.1\ \mathrm{fm}^2$, i.e. $\langle r^2_{\text{constituent quark}}\rangle \ll \langle R^2_{\text{hadron}}\rangle$, see [1 – 3], Chapter 1, and references therein.

2. Systematization of mesons in terms of constituent quarks. The systematization of mesons supports the idea of constituent quarks. A decade ago, a considerable progress was reached in the discovery of highly excited meson states in the mass region 1950–2400 MeV, that allowed us to systematize $q\bar{q}$-meson states on the (n, M^2) and (J, M^2) planes, n being the radial quantum number of a $q\bar{q}$ system with mass M and spin J. The $q\bar{q}$ states, $n^{2S+1}L_J q\bar{q}$, $M \lesssim$ 2400 MeV, fill in the following (n, M^2) trajectories, Figs.1, 2:

$$
\begin{aligned}
&{}^1S_0 \;\to\; \pi(10^{-+}),\ \eta(00^{-+});\\
&{}^3S_1 \;\to\; \rho(11^{--}),\ \omega(01^{--})/\phi(01^{--});\\
&{}^1P_1 \;\to\; b_1(11^{+-}),\ h_1(01^{+-});\\
&{}^3P_J \;\to\; a_J(1J^{++}),\ f_J(0J^{++}),\ J = 0, 1, 2;\\
&{}^1D_2 \;\to\; \pi_2(12^{-+}),\ \eta_2(02^{-+});\\
&{}^3D_J \;\to\; \rho_J(1J^{--}),\ \omega_J(0J^{--})/\phi_J(0J^{--}),\ J = 1, 2, 3;\\
&{}^1F_3 \;\to\; b_3(13^{+-}),\ h_3(03^{+-});\\
&{}^3F_J \;\to\; a_J(1J^{++}),\ f_J(0J^{++}),\ J = 2, 3, 4. \qquad (1)
\end{aligned}
$$

In Fig.2, one can see the states which, being superfluous for the $q\bar{q}$ trajectories, are flavour-blind: they are scalar and tensor glueballs [1, 4], see also the K-matrix analyses [2, 3].

3. Spectral integral equation for $q\bar{q}$ mesons and confinement. The systematization of mesons as $q\bar{q}$ states (Figs.1, 2) tells us that in low-energy physics we can treat constituent quarks as standard particles but with the account for their confinement. If we wish to forbid quarks to fly away in hadronic processes, it is worth appealing to quantum mechanics. Quantum mechanics show us the way to prevent quarks to leave the confinement trap: for the $q\bar{q}$ system one should introduce a barrier at $r \sim r_{\text{hadron}}$. To deal with highly excited hadrons we need a relativistic generalization of the calculation technique – the best way, in our opinion, is to use the dispersion relation method. This point was discusseed in [1, 5].

3.1. Spectral integral and Bethe–Salpeter equations. The relativistic generalization of the quark model is performed rather often in terms of the Bethe–Salpeter

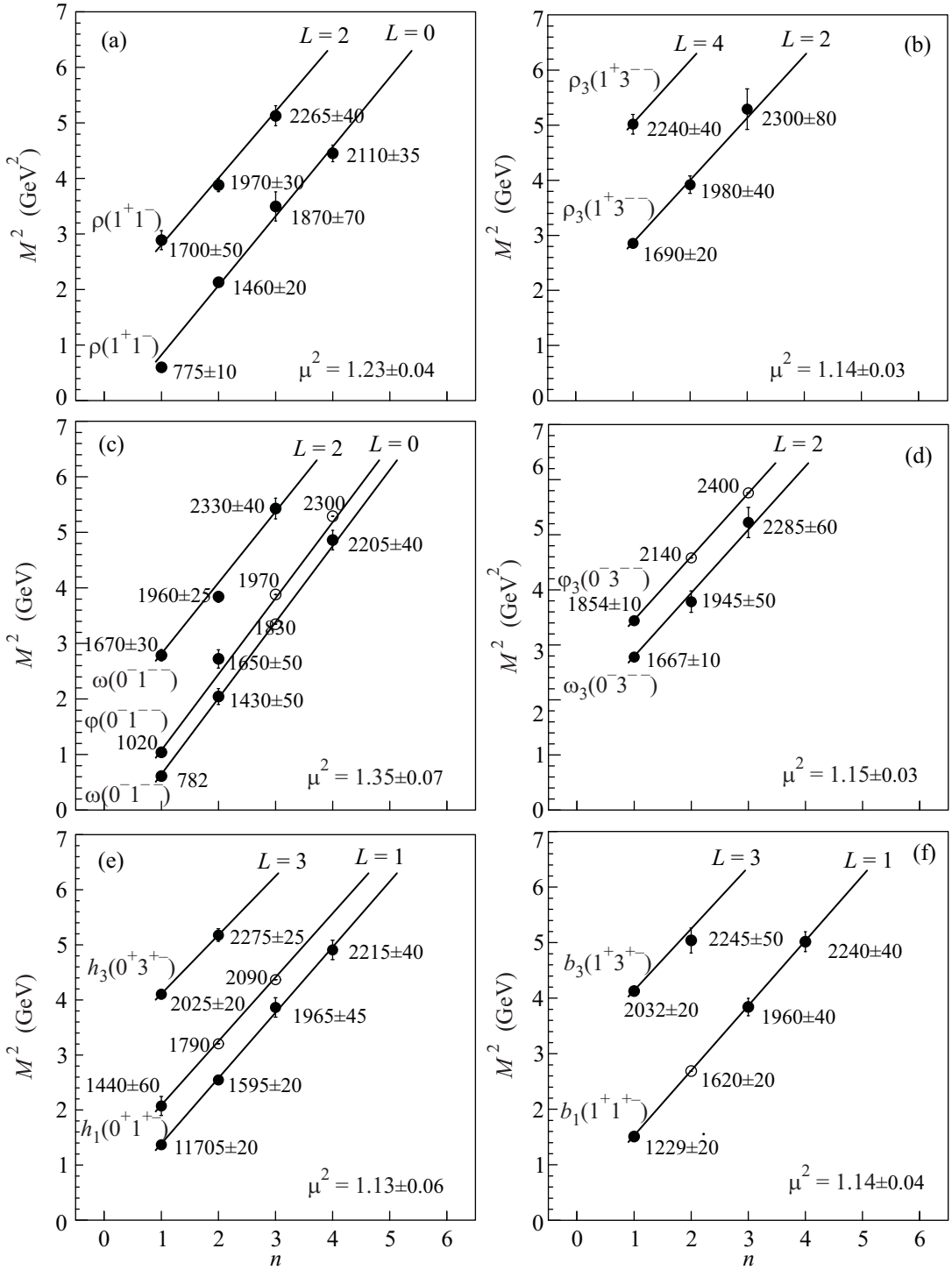

Fig.1. Trajectories for $(C = -)$ meson states on the (n, M^2) plane. Black dots mark observed states, open circles stand for predicted states. Isoscalar states have two flavour components each, $n\bar{n} = (u\bar{u} + d\bar{d})/\sqrt{2}$ and $s\bar{s}$, this doubles the number of trajectories

equation. The Bethe–Salpeter equation is based on the summation of a set of ladder diagrams in the Feynman technique, the interaction is usually assumed to be instantaneous. The spectral integral technique applied to the description of the quark–antiquark systems is a variant of the dispersion N/D method. In refs. [5], the method has been modified to describe quark–antiquark systems.

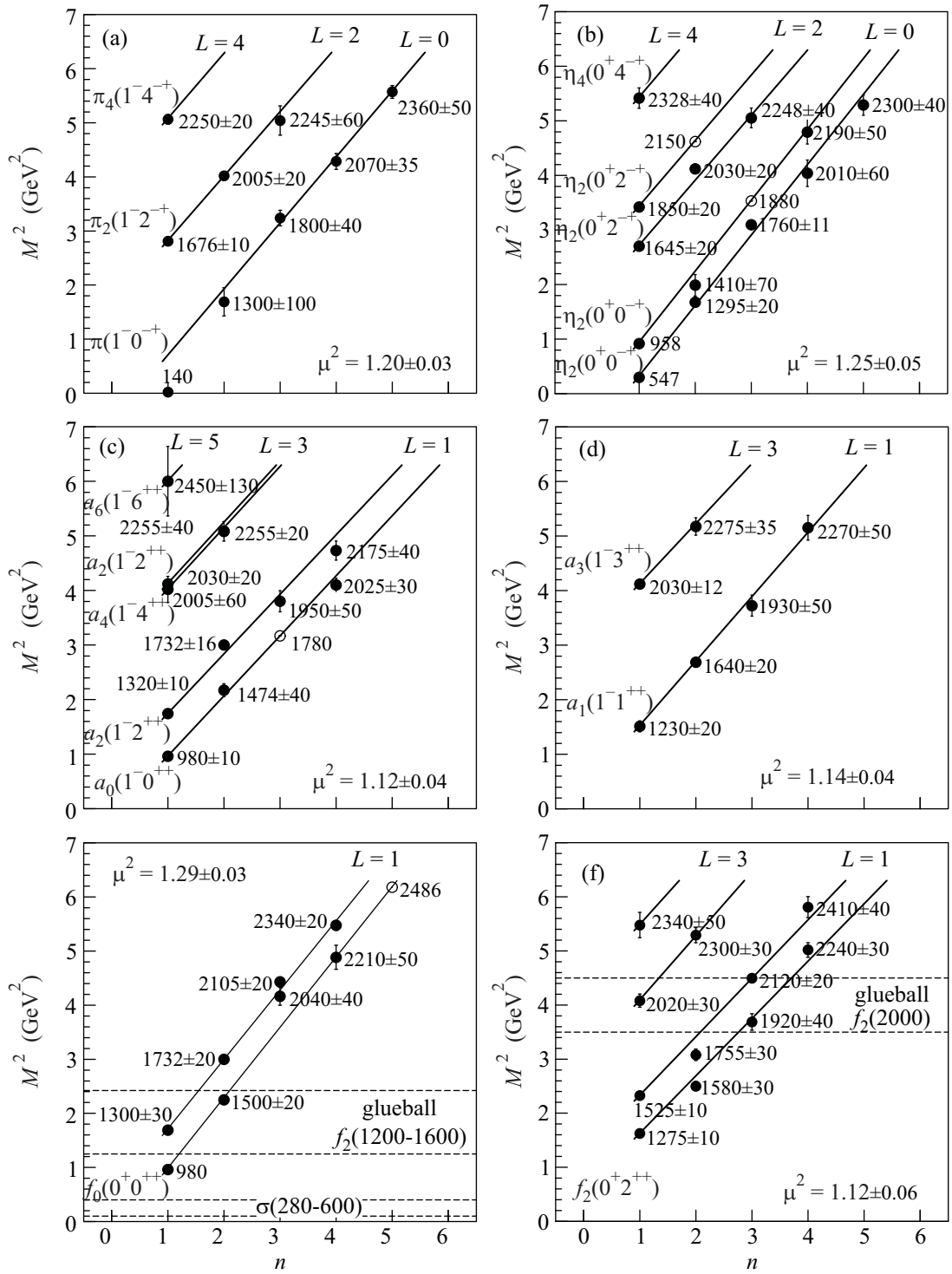

Fig.2. Trajectories for $(C = +)$ meson states on the (n, M^2) plane. Open circles stand for predicted states. States with $J = L \pm 1$ have two components: at fixed J there are states with $L - 1$ and $L + 1$, so one may assert the doubling of the trajectory at fixed J, for example, for $(I, 1^{--})$ and $(I, 2^{++})$. The bands restricted by dotted lines show mass regions of scalar $(f_0(1200 - 1600))$ and tensor $(f_2(2000))$ glueballs; the band $\sigma(280 - 600)$ shows mass region of the σ meson

3.2. Bethe–Salpeter equations and zoo-diagrams. We should emphasize an important difference between the standard Bethe–Salpeter equation and that written in terms of the spectral integral. In the dispersion relation technique the constituents in the intermediate state are mass-on-shell, $k_i^2 = m^2$, while in the Feynman tech-

nique, which is used in the Bethe–Salpeter equation, $k_i^2 \neq m^2$. So, in the spectral integral equation, when the high-spin structures are calculated, we have a simple numerical factor $k_i^2 = m^2$, while in the Feynman technique one has $k_i^2 = m^2 + (k_i^2 - m^2)$. The first term here provides us with a contribution similar to that used in the spectral integrals, while the second term cancels one of denominators in the kernel of Bethe–Salpeter equation. This results in the existence of penguin or tadpole type diagrams – in [1] they are called zoo-diagrams. A particular feature of the spectral integral technique is the exclusion of zoo-diagrams from the equation, so the found mesons are pure $q\bar{q}$ states.

3.3. Spectral integral equation for the $q\bar{q}$ system: a simple example. Here, we present a simple example of spectral integral equation for the $q\bar{q}$ system – we consider the $(J^P = 0^-)$ system. The graphical representation of the equation is given in Fig.3. The equation for

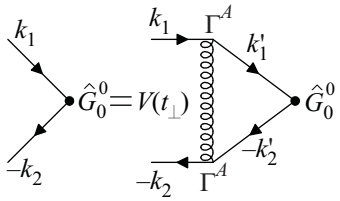

Fig.3. Spectral integral equation for $q\bar{q}$ meson

the pseudoscalar-state vertex $g^{(S,L,J)}(s)$ with the quark–antiquark spin $S = 0$, angular momentum $L = 0$, meson spin $J = 0$ and radial quantum number $n = 1, 2, 3, ...$ reads:

$$\bar{\psi}(-k_2) i\gamma_5 g^{(0,0,0)}(s)\psi(k_1) = \\ = \int \frac{d^3k'}{(2\pi)^3 k_0'} \bar{\psi}(-k_2) V(t_\perp) \Gamma^A(-\hat{k}_2' + m) \times \\ \times \frac{i\gamma_5 g^{(0,0,0)}(s')}{s' - M^2} (\hat{k}_1' + m)\Gamma_A]\psi(k_1). \qquad (2)$$

In the fit of $q\bar{q}$ states [5], we have used two types of Interactions – scalar and vector ones: $\Gamma_A = 1$, and $\Gamma_A = \gamma_\mu$, $V(t_\perp)$ describes the interaction without retardation.

The vertex and wave function for the $(S = 0,\ L = 0,\ J = 0)$ state are determined as follows

$$\hat{G}^{(0,0,0)}(k_\perp) = i\gamma_5, \quad \hat{\Psi}_n^{(0,0,0)}(s) = \\ = \hat{G}^{(0,0,0)}(k_\perp) \frac{g_n^{(0,0,0)}(s)}{s - M_n^2} = \hat{G}^{(0,0,0)}(k_\perp)\psi_n^{(0,0,0)}(s). \quad (3)$$

Equations for other mesons can be found in [1, 5].

3.4. Calculation results for $q\bar{q}$ mesons: masses and wave functions. In [5], by fitting to mass values of mesons lying on the (n, M^2) trajectories, the interaction and wave functions were found:

$$L = 0 : \pi(0^{-+}),\ \rho(1^{--}),\ \omega(1^{--}),\ \phi(1^{--}), \qquad (4)$$
$$L = 1 : a_0(0^{++}),\ a_1(1^{++}),\ a_2(2^{++}),$$
$$b_1(1^{+-}),\ f_2(2^{++}),$$
$$L = 2 : \pi_2(2^{-+}),\ \rho(1^{--}),\ \rho_3(3^{--}),$$
$$\omega(1^{--}),\ \omega_3(3^{--}),\ \phi_3(3^{--}),$$
$$L = 3 : a_2(2^{++}),\ a_3(3^{++}),\ a_4(4^{++}),$$
$$b_3(3^{+-}),\ f_2(2^{++}),\ f_4(4^{++}),$$
$$L = 4 : \rho_3(3^{--}),\ \pi_4(4^{-+}).$$

The linearity of trajectories in the (n, M^2) plane (experimentally – up to large n values, $n \leq 7$) provides us with the t-channel singularity $V_{\rm conf} \sim 1/q^4$ or, in the coordinate representation, $V_{\rm conf} \sim r$. In the coordinate representation the confinement interaction can be written in the following potential form [1]: $V_{\rm conf} = (I \otimes I)\, b_S\, r + (\gamma_\mu \otimes \gamma_\mu)\, b_V\, r$, with $b_S \simeq -b_V \simeq 0.15\,{\rm GeV}^{-2}$. The spectral integral equation for the $q\bar{q}$-meson wave function was solved by introducing a cut-off into the interaction: $r \to re^{-\mu r}$. The cut-off parameter is small, $\mu \sim 1{-}10\,{\rm MeV}$: if μ changes in this interval, the $q\bar{q}$ levels with $n \leq 7$ remain practically the same.

In general, keeping in mind that in the framework of spectral integral method (as in the dispersion technique) the total energy is not conserved, we have to write $t_\perp = (k_1^\perp - k_1'^\perp)_\mu (-k_2^\perp + k_2'^\perp)_\mu$. Recall that k_1 and k_2 are the momenta of the initial quark and antiquark, while k_1' and k_2' are those after the interaction. The index $\perp$ means that we use components perpendicular to the total momentum p of the initial state and to p' of the final state. One can write for quarks with equal masses:

$$r^N e^{-\mu r} = \int \frac{d^3q}{(2\pi)^3} e^{-i\mathbf{qr}} I_N(t_\perp),$$

$$I_N(t_\perp) = \frac{4\pi(N+1)!}{(\mu^2 - t_\perp)^{N+2}} \times \qquad (5)$$
$$\times \sum_{n=0}^{N+1} \left(\mu + \sqrt{t_\perp}\right)^{N+1-n} \left(\mu - \sqrt{t_\perp}\right)^n.$$

The confinement singularity $(\mu \to 0)$ in the crossing white channel could behave as $1/s^2$, but the transition into $\pi\pi$ channel splits it into two poles $1/s^2 \to g_1/(s - M_1^2) + g_2/(s - M_2^2)$. One pole reveals itself as the σ meson, see Fig.2, another pole dives deeply into the complex M^2 plane (for more detail see [1], Capter 2).

4. Radiative decays of hadrons and photon wave function. Considering radiative decays of hadrons in the spectral integral technique, we should

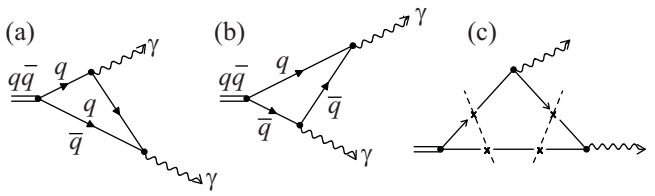

Fig.4. Diagrams for the two-photon decay of a $q\bar{q}$ state with the emission of a photon in the intermediate state by a quark (a) and an antiquark (b). Figure (c) demonstrates the cuttings of the diagram (a) for the calculation of discontinuity in the double spectral integral

take into account two subprocesses shown in Fig.4 for the two-photon decay of a $q\bar{q}$ state: the emission of a photon in the intermediate state by a quark (a) or an antiquark (b) and subsequant annihilation $q\bar{q} \to \gamma$. Moreover, one should take into account the initial and final state interactions of quarks. These interactions determine the quark wave functions of meson and photon.

4.1. Photon wave function. The photon wave function has two components: the soft and hard ones. The hard component is related to the point-like vertex $\gamma \to q\bar{q}$, it is responsible for the production of a quark–antiquark pair at high photon virtuality. The soft component is responsible for the production of low-energy quark–antiquark vector states such as ρ^0, ω, $\phi(1020)$ and their excitations.

The photon wave function depends on the invariant energy squared of the $q\bar{q}$ system:

$$\psi_{\gamma^*(Q^2)\to q\bar{q}}(s) = \frac{G_{\gamma\to q\bar{q}}(s)}{s+Q^2}.$$

Here, $G_{\gamma\to q\bar{q}}(s)$ is the vertex for the transition of a photon into $q\bar{q}$ state, and $(s+Q^2)^{-1}$ is the wave function denominator ($q^2 = -Q^2$).

In [6], the photon wave function has been found under the assumption of the vertex universality for u and d quarks, $G_{\gamma\to u\bar{u}}(s) = G_{\gamma\to d\bar{d}}(s) \equiv G_\gamma(s)$. It looks rather trustworthy because of the degeneracy of trajectories ρ and ω states.

4.2. Ratio $R(s) = \sigma(e^+e^- \to hadrons)/\sigma(e^+e^- \to \mu^+\mu^-)$. In Fig.5, we present the ratio $R(s) = \sigma(e^+e^- \to hadrons)/\sigma(e^+e^- \to \mu^+\mu^-)$ which is determined by the photon wave function for non-strange and strange quarks. A detailed description of parameters is given in [6].

At high energies but below the open charm production, $E_{e^+e^-} = \sqrt{s} < 3.7$ GeV, the ratio $R(s)$ is determined by the sum of quark charges squared in the transition $e^+e^- \to \gamma^* \to u\bar{u} + d\bar{d} + s\bar{s}$ multiplied by the factor $N_c = 3$ that gives us $R(s) = 2$ at large energies.

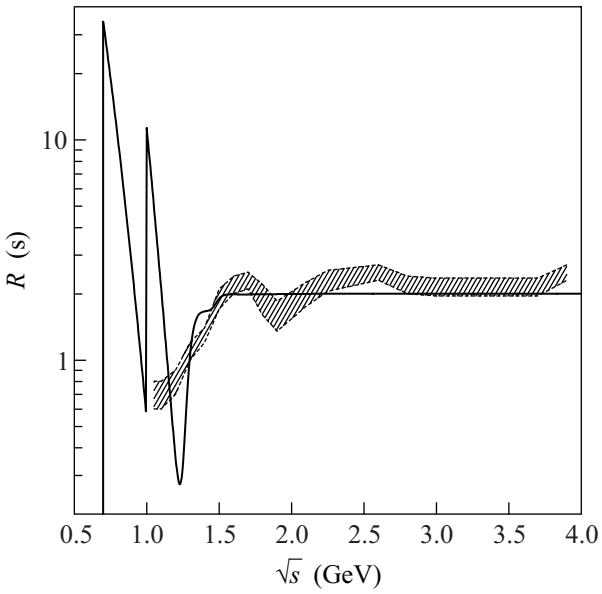

Fig.5. The ratio $R(s) = \sigma(e^+e^- \to hadrons)/\sigma(e^+e^- \to \mu^+\mu^-)$ at energies below the open charm production: the result of the fit is shown by solid line, while hatched area present the experimental estimations

4.3. Partial decay widths $\omega, \rho^0, \phi \to e^+e^-$. Partial decay widths $\omega, \rho^0, \phi \to e^+e^-$ are determined by the process shown in Fig.6. This diagram depends on wave

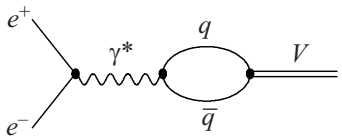

Fig.6. Production of a vector $q\bar{q}$ state in the e^+e^- annihilation: this process was used in [6] for the determination of $G_{\gamma\to q\bar{q}}(s)$

functions (or vertices) of the photon and decaying meson. The calculation leads to the following results:

$$\begin{aligned}
&\Gamma^{\rm calc}_{\rho^0\to e^+e^-} = 7.50,\ \Gamma^{\rm exp}_{\rho^0\to e^+e^-} = 6.77 \pm 0.32,\\
&\Gamma^{\rm calc}_{\omega\to e^+e^-} = 0.796,\ \Gamma^{\rm exp}_{\omega\to e^+e^-} = 0.60 \pm 0.02,\\
&\Gamma^{\rm calc}_{\phi\to e^+e^-} = 1.33,\ \Gamma^{\rm exp}_{\phi\to e^+e^-} = 1.32 \pm 0.06.
\end{aligned} \qquad (6)$$

4.4. Results of the calculation of transition form factors $\pi^0, \eta, \eta' \to \gamma(Q^2)\gamma$. In Fig.7 one can see the calculation results for transition form factors $\pi^0, \eta, \eta' \to \gamma(Q^2)\gamma$. Here, as previously, we see a good description of data. The photon wave function, which determines these results, is presented in [1, 6] together with corresponding formulae for amplitudes in the spectral integral technique.

5. Decays of $q\bar{q}$ mesons into $\gamma\pi$. To study the confinement mechanism, it is important to know not

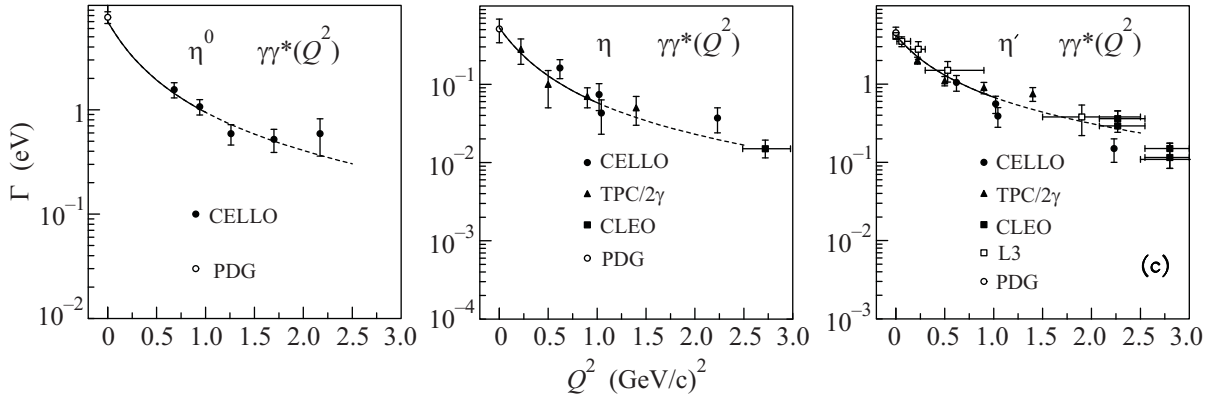

Fig.7. Data for $\pi^0 \to \gamma\gamma^*$, $\eta \to \gamma\gamma^*$ and $\eta' \to \gamma\gamma^*$ *vs* calculated curves

only the structure of forces, which keep quarks inside the region ~ 1 fm, but also to know the way they escape the confinement trap. Here we consider the processes $\rho, \omega \to \gamma\pi$.

In the radiative decays $\rho, \omega \to \gamma\pi$ we face two mechanisms: a bremsstrahlung emission of a photon $q \to \gamma + q$ with a subsequent transition $q\bar{q} \to \pi$ and a bremsstrahlung-type emission of a pion $q \to \pi + q$ with a subsequent annihilation $q\bar{q} \to \gamma$, see Fig.8.

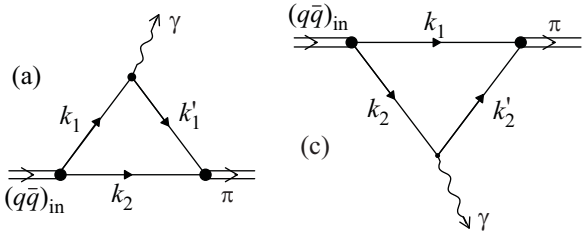

Fig.8. The $\rho \to \pi\gamma$ process

Therefore, the key point in the calculation of the $\rho, \omega \to \gamma\pi$ decays is to know the $q\bar{q}$ wave functions of the pion and vector mesons, ρ and ω, as well as the wave function of the photon $\gamma \to q\bar{q}$. The pion bremsstrahlung constant for the process $q \to \pi q$ is determined by the pion-nucleon coupling constant $g^2_{\pi\pi N}/(4\pi) \simeq 14$. All factors in processes of Fig.8 being known, we have calculated partial widths – they coincide with the observed ones: $\Gamma^{(\exp)}_{\rho^\pm \to \gamma\pi^\pm} = 68 \pm 30$ keV, $\Gamma^{(\exp)}_{\rho^0 \to \gamma\pi^0} = 77 \pm 28$ keV, $\Gamma^{(\exp)}_{\omega \to \gamma\pi^0} = 776 \pm 45$ keV.

6. Decay $\rho \to \pi\pi$. The next step in the study of meson decay is to consider the $\rho \to \pi\pi$ reaction. The study of $\rho \to \pi\pi$ demonstrates that here, apart from the pion bremsstrahlung processes (Figs.9a, b), we should include into consideration a new one, namely, the Gribov confinement quark exchange [7], Figs.9c.

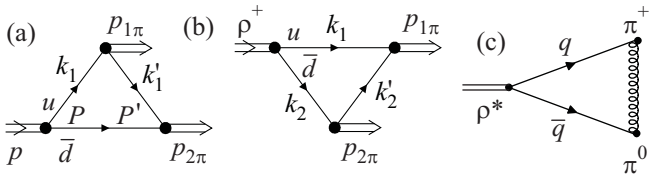

Fig.9. The $\rho^+ \to \pi^+\pi^0$ process: a,b) with a bremsstrahlung-type pion emission and c) with the $q\bar{q} \to \pi\pi$ transition realized owing to the t-channel confinement singularity with fermion quantum numbers

The Gribov's transition $q\bar{q} \to \pi\pi$ is necessary for the numerical description of the $\rho(775) \to \pi\pi$-decay width. However, the structure of the $q\bar{q} \to \pi\pi$ amplitude is not determined unambiguously – there remains a freedom in choosing the singularity type. We have analysed in [8] some possibilities. Doing so on the basis of experimental data for $\rho(775) \to \pi\pi$, we estimate the contribution of the amplitude $q\bar{q} \to \pi\pi$ for different versions of the interaction.

The decay processes $\rho \to \pi\pi$ (to be definite, we consider $\rho^+ \to \pi^0\pi^+$) are demonstrated in Fig.9. While the processes of Fig.9a,b do not differ in their structure from those shown in Fig.4 and Fig.8, the process of Fig.9c is principally different. In the bremsstrahlung-type processes one of the particles (the photon or the pion) is emitted by a constituent quark when it is inside a "bag". Further, two quarks form a particle: a pion or a photon – obviously, with the participation of the confinement interaction.

The calculation of amplitudes demonstrates that for the quark confinement principally decisive is the singular interaction – just because of this interaction the quark singularities are absent in the amplitudes of Figs.9a,b for the $\rho \to \pi\pi$ decay. Correspondingly, the amplitudes are real in the physycal region. The Gribov's singularity plays another and very important role. The matter

is that the bremsstrahlung-type radiation of pions (i.e. the radiation coming from the region of the confinement trap) is rather large. Were it the only possible process, it would lead to a broad decay width of the ρ meson, $\sim$ 2000 MeV. But the process with Gribov's singularity, Fig.9c, prevents such a "smearing" – it looks like the only way to keep the ρ meson as a comparatively narrow state.

7. Self-energy part $\rho \to \pi\pi \to \rho$. We have calculated masses and wave functions of $q\bar{q}$ states in the infinite-wall approach (the requirement $\mu \to 0$). It means that in the calculation of widths we neglect the inverse influence of the $\pi\pi$ channel upon the characteristics of the ρ meson. The reliability of such an approach was discussed in [8].

To this aim, we take into account the $\pi\pi$ channel. The corresponding two-component equation is shown in a graphical form in Fig.10:

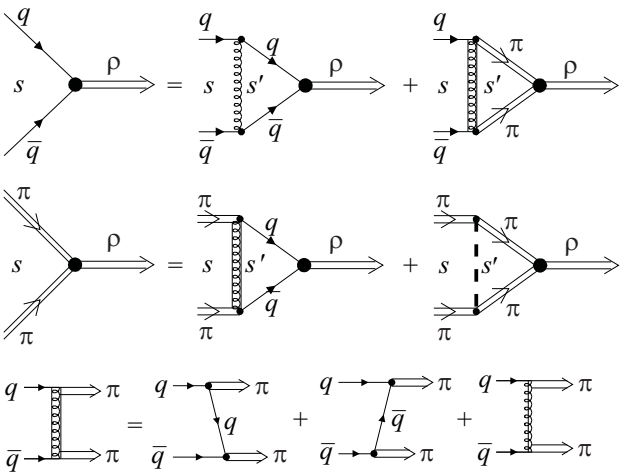

Fig.10. Graphical representation of two-channel ($q\bar{q}$, $\pi\pi$) equations for the ρ meson

The following simplifying steps can be made:

(i) the second term in the right-hand side of the ($q\bar{q} \to \rho$) equation may be considered as a perturbative correction, because the ρ-meson width is not large.

(ii) the last term in the equation $\pi\pi \to \rho$ can be neglected due to the smalness of the $\pi\pi$ interaction in the ρ-meson region.

In this way, we have a standard one-channel equation for $\rho_{(q\bar{q})}$ shown in Fig.11a where $\rho_{(q\bar{q})}$ is a pure $q\bar{q}$ state. The $\pi\pi$ channel reveals itself in the self-energy part $\rho_{(q\bar{q})} \to \pi\pi \to \rho_{(q\bar{q})}$, see Fig.11b. Denoting this self-energy part as $B(s, M^2_{\rho(q\bar{q})})$, one transforms the propagator of a pure $q\bar{q}$ state as follows:

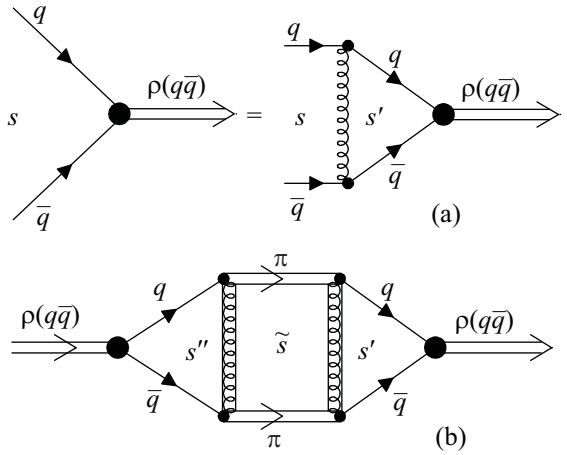

Fig.11. Graphical representation of a) the equation for pure $q\bar{q}$ state $\rho(q\bar{q})$ and b) the self-energy part $B(s, M^2_{\rho(q\bar{q})})$, which determines the admixture of the $\pi\pi$ component in the ρ meson

$$\frac{\sum\limits_a \epsilon^{(a)}_\nu \epsilon^{(a)+}_{\nu'}}{M^2_{\rho(q\bar{q})} - s} \to \frac{\sum\limits_a \epsilon^{(a)}_\nu \epsilon^{(a)+}_{\nu'}}{M^2_{\rho(q\bar{q})} - s - B(s, M^2_{\rho(q\bar{q})})} =$$

$$= \frac{\sum\limits_a \epsilon^{(a)}_\nu \epsilon^{(a)+}_{\nu'}}{M^2_{\rho(q\bar{q})} - \mathrm{Re}B(s, M^2_{\rho(q\bar{q})}) - s - i\,\mathrm{Im}B(s, M^2_{\rho(q\bar{q})})} \simeq$$

$$\simeq \frac{\sum\limits_a \epsilon^{(a)}_\nu \epsilon^{(a)+}_{\nu'}}{M^2_\rho - s - i\,M_\rho \Gamma_\rho}, \qquad (7)$$

where

$$M^2_\rho = M^2_{\rho(q\bar{q})} - \mathrm{Re}\,B(M^2_\rho, M^2_{\rho(q\bar{q})}) = (0.770)^2 \mathrm{GeV}^2,$$

$$M_\rho \Gamma_\rho = \mathrm{Im}\,B(M^2_\rho, M^2_{\rho(q\bar{q})}). \qquad (8)$$

The fit [5] tells us that $M^2_\rho \simeq M^2_{\rho(q\bar{q})}$, thus providing us with a rather small value of the mass shift in the region of $s \sim M^2_\rho$:

$$\mathrm{Re}\,B(M^2_\rho, M^2_{\rho(q\bar{q})}) \simeq 0.$$

7.1 Self-energy part $B(s, M^2_{\rho(q\bar{q})})$ and confinement. The self-energy part of a pure $q\bar{q}$ state reads:

$$B(s, M^2_{\rho(q\bar{q})}) = \int\limits_{4M^2_\pi}^{\infty} \frac{d\tilde{s}}{\pi} \frac{\mathrm{Im}B(\tilde{s}, M^2_{\rho(q\bar{q})})}{\tilde{s} - s - i0}, \qquad (9)$$

$$\mathrm{Im}B(s, M^2_{\rho(q\bar{q})}) = \frac{1}{48\pi} \sqrt{\frac{(s - 4M^2_\pi)^3}{s}} \times$$

$$\times \left(2A \left(\triangle^{\pi^+}_{\pi^0}; s, M^2_\rho \right) + A \left(\sphericalangle^{\pi^+}_{\pi^0}; s, M^2_\rho \right) \right)^2.$$

We should emphasize that, according to calculations [8], the amplitudes of the production of two pions, $A\left(\triangle^{\pi^+}_{\pi^0}; s, M^2_\rho\right)$ and $A\left(\triangleleft^{\pi^+}_{\pi^0}; s, M^2_\rho\right)$, have no imaginary parts in the $\mu \to 0$ limit, despite the presence of the $q\bar{q}$ state in intermediate states. This means the quark confinement.

The only particles flying away are pions: the threshold singularity in (9) at $s = 4M^2_\pi$ manifests just this fact.

Frank acknowledgement is done to the RFBF grant # 07-02-02-01197a for the support of papers carried out in 2007–2009 years.

1. A. V. Anisovich, V. V. Anisovich, J. Nyiri et al., *Mesons and Baryons. Systematization and Methods of Analysis*, World Scientific, Singapore, 2008.
2. V. V. Anisovich and A. V. Sarantsev, Eur. Phys. J. A **16**, 229 (2003); JETP Letters **81**, 417 (2005); Yad. Fiz. **72**, 1950 (2009) [Phys. At. Nucl. **72**, 1889 (2009)]; Yad. Fiz. **72**, 1981 (2009) [Phys. At. Nucl. **72**, 1920 (2009)]; Int. J. Mod. Phys. A **24**, 2481 (2009).
3. V. V. Anisovich, UFN **174**, 49 (2004) [Physics-Uspekhi, **47**, 45 (2004)].
4. V. V. Anisovich, Pis'ma v JETP **80**, 845 (2004) [JETP Letters **80**, 715 (2004)]; V. V. Anisovich and A. V. Sarantsev, Pis'ma v JETP **81**, 531 (2005) [JETP Letters **81**, 417 (2005)]; V. V. Anisovich, M. A. Matveev, J. Nyiri, and A. V. Sarantsev, Int. J. Mod. Phys. A **20**, 6327 (2005).
5. V. V. Anisovich, L. G. Dakhno, M. A. Matveev et al., Yad. Fiz. **70**, 68 (2007) [Phys. Atom. Nucl. **70**, 63 (2007)]; Yad. Fiz. **70**, 392 (2007) [Phys. Atom. Nucl. **70**, 364 (2007)], Yad. Fiz. **70**, 480 (2007) [Phys. Atom. Nucl. **70**, 450 (2007)].
6. V. V. Anisovich, D. I. Melikhov, and V. A. Nikonov, *Phys. Rev.* D **52**, 5295 (1995); A. V. Anisovich, V. V. Anisovich, L. G. Dakhno et al., Yad. Fiz. **68**, 1892 (2005) [Phys. Atom. Nucl. **68**, 1830 (2005)].
7. V. N. Gribov, *Theory of Quark Confinement*, World Scientific, Singapore, 2001.
8. A. V. Anisovich, V. V. Anisovich, L. G. Dakhno et al., Yad. Fiz. **72**, 1572 (2009) [Phys. Atom. Nucl. **72**, 1550 (2009)], J. Phys. G: Nucl. Part. Phys. **37**, 025004 (2010); Yad. Fiz. **73**, 488 (2010) [Phys. Atom. Nucl. **73**, 462 (2010)]; A. V. Anisovich, V. V. Anisovich, M. A. Matveev et al., Yad. Fiz. **73**, 1294 (2010) [Phys. Atom. Nucl.**73**, 1254 (2010)].